

SUPPLEMENTARY INFORMATION

A Hybridized Local and Charge Transfer Excited State for Solution-Processed Non-doped Green Electroluminescence Based on Oligo(*p*-phenyleneethynylene)

Hakan Usta^{1*}, Dilek Alimli², Resul Ozdemir¹, Emine Tekin³, Fahri Alkan¹, Rifat Kacar³, Ahu Galen Altas³, Salih Dabak³, Ayşe Gül Gürek², Evren Mutlugun⁴, Ahmet Faruk Yazici¹, Ayse Can¹

¹ Department of Materials Science and Nanotechnology Engineering, Abdullah Gül University, 38080 Kayseri, Turkey.

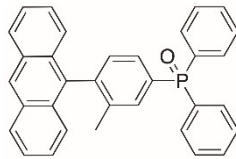
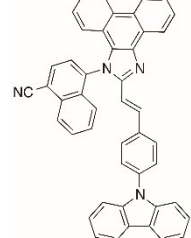
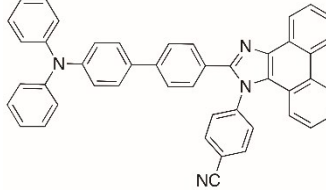
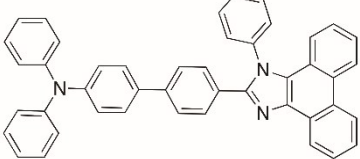
² Department of Chemistry, Gebze Technical University, 41400 Gebze, Kocaeli, Turkey.

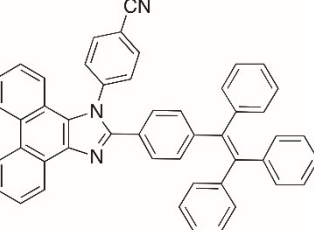
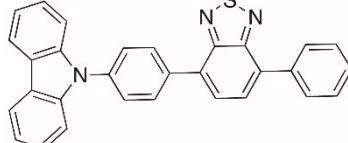
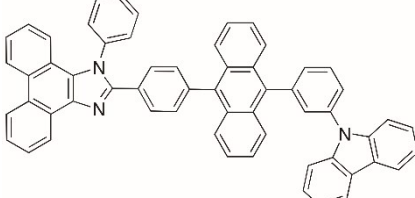
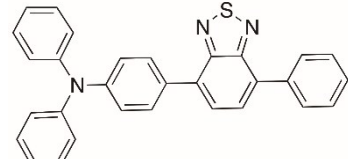
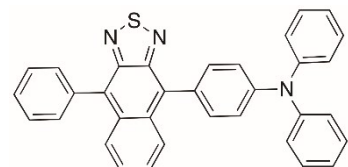
³ The Scientific and Technological Research Council of Turkey (TUBITAK)-Marmara Research Center (MAM), 41470 Gebze, Kocaeli, Turkey.

⁴ Department of Electrical and Electronics Engineering, Abdullah Gül University, 38080 Kayseri, Turkey.

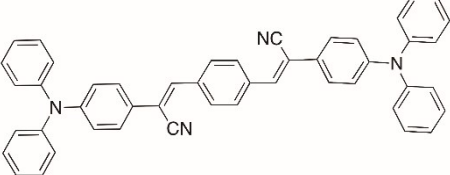
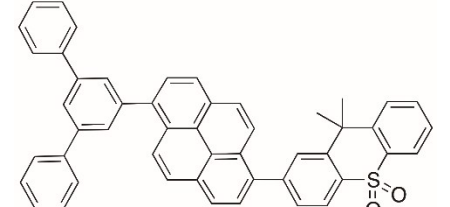
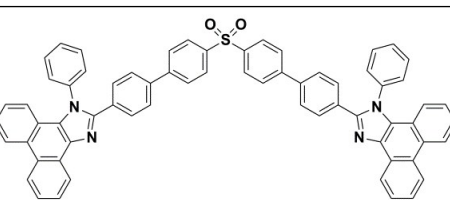
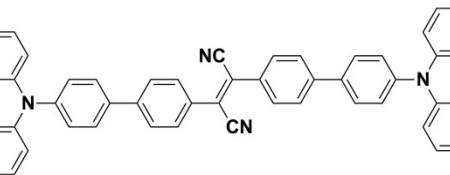
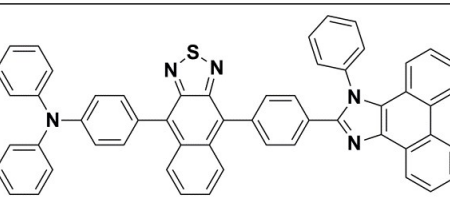
*Address correspondence to: hakan.usta@agu.edu.tr

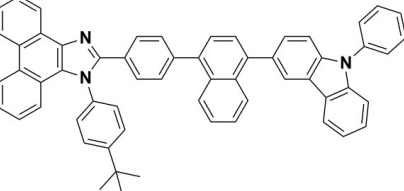
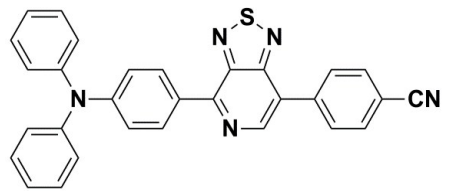
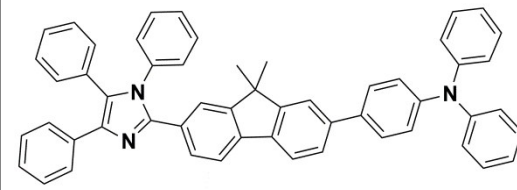
Table S1. The molecular structures, photophysical characteristics (PLQY(solution/solid-state)), and OLED device structures and performances (EQE_{max}, CE_{max}, CIE(x,y), and radiative exciton yield (η_r (%))) of previously reported fluorescent small molecules utilizing hot-exciton mechanisms.

Molecular Structure	EQE _{max} (%) (η_r (%))	CE _{max} (cd/A)	PLQY solution	PLQY solid state	CIE (x,y)	Device Structure	Notes	Reference
	7.03 (72)	24.21	89	49	(0.26, 0.62)	ITO/MoO ₃ /NPB/An-9-MePo:C545T/TPBi/LiF/Al	Doped device, green emission, vacuum-deposited emissive layer.	Yu et al. ¹
	3.15 (32.14)	2.56	52	49	(0.15, 0.07)	ITO/ NPB/SPNCN-Cz /TPBi/LiF/Al	Non-doped device, deep-blue emission, vacuum-deposited emissive layer.	Jayabharathi et al. ²
	7.8 (97)	10.5	79	40	(0.16, 0.16)	ITO/ PEDOT:PSS/NPB/TC TA/TBPMCN /TPBi/LiF/Al	Non-doped device, blue emission, vacuum-deposited emissive layer.	Zhang et al. ³
	5.02 (-)	5.66	90	90	(0.15, 0.11)	ITO/MoO ₃ /NPB/TCTA/TPA-PPI /TPBi/LiF/Al	Non-doped device, deep-blue emission, vacuum-deposited emissive layer.	Li et al. ⁴

	7.16 (48.1)	18.46	50	59.5	(0.211, 0.402)	ITO/HATCN /TAPC /TCTA/ppCTPI /TmPyPB/LiF/Al	Non-doped device, blue emission, vacuum-deposited emissive layer.	Zhang et al. ⁵
	6.95 (48)	23.99	59.9	75	(0.34, 0.60)	ITO/ PEDOT:PSS/NPB/TC TA/CzP-BZP /TPBi/LiF/Al	Non-doped device, green emission, vacuum-deposited emissive layer.	Wang et al. ⁶
	10.5 (-)	12.37	76	48	(0.15, 0.13)	ITO/ PEDOT:PSS/TCTA/P AC /TPBi/LiF/Al	Non-doped device, blue emission, vacuum-deposited emissive layer.	Xu et al. ⁷
	3.8 (42)	8.84	-	45	(0.55, 0.45)	ITO/ PEDOT:PSS/NPB/TC TA/TPA-BZP /TPBi/LiF/Al	Non-doped device, orange emission, vacuum-deposited emissive layer.	Li et al. ⁸
	2.8 (93)	1.3	-	-	(0.67, 0.32)	ITO/MoO ₃ /NPB/TCT A/TPA-NZP /TPBi/LiF/Al	Non-doped device, deep-red emission, vacuum-deposited emissive layer.	Li et al. ⁹

	1.54 (48)	-	-	-	(0.69, 0.30)	ITO/ PEDOT:PSS/NPB/TC TA/PTZ-BZP /TPBi/LiF/Al	Non-doped device, deep-red emission, vacuum- deposited emissive layer.	Yao et al. ¹⁰
	2.18 (85)	2.69	10	13	(0.15, 0.18)	ITO/ PEDOT:PSS/NPB/ TPMCN/TPBi/LiF/Al	Non-doped device, blue emission, vacuum- deposited emissive layer.	Zhang et al. ¹¹
	3.89 (46.3)	2.11	100	42	(0.15, 0.05)	ITO/MoO ₃ /NPB/TCT A/mpt/TPBi/LiF/Al	Non-doped device, deep-blue emission, vacuum- deposited emissive layer.	Li et al. ¹²
	6.80 (75.6)	19.58	90	28.1	-	ITO/NPB/MADN:BD PACS/Bphen/Liq/Al	Doped device, green emission, vacuum- deposited emissive layer.	Yuan et al. ¹³
	2.0 (-)	6.8	1.6	12.9	(0.365, 0.602)	ITO/HATCN/NPB/M ADN: α -CN- APV/TPBi/LiF/Al	Doped device, green emission, vacuum- deposited emissive layer.	Li et al. ¹⁴

	5.3 (-)	14.6	86.9	53.9	(0.495, 0.499)	ITO/HATCN/NPB/M ADN: β -CN-APV/TPBi/LiF/Al	Doped device, yellow emission, vacuum-deposited emissive layer.	Li et al. ¹⁴
	10.5 (-)	11.1	51	39	(0.152, 0.065)	ITO/HATCN/HATCN :TAPC/TPP-TXO ₂ /26DCzPPy: TPP-TXO ₂ /LiF/Al	Doped device (double emissive layer), deep-blue emission, vacuum-deposited emissive layer.	Fu et al. ¹⁵
	6.80 (47)	4.64	~100	72	(0.152, 0.077)	ITO/MoO ₃ /TCTA/PM SO:CBP/TPBi/LiF/Al	Doped device, deep blue emission, vacuum-deposited emissive layer.	Tang et al. ¹⁶
	2.58 (39)	0.96	94.9	33	(0.673, 0.324)	ITO/PEDOT:PSS/NPB/TPATCN/BCP/AlQ ₃ /LiF/Al	Non-Doped device, near-infrared emission, vacuum-deposited emissive layer.	Han et al. ¹⁷
	6.83 (82)	3.45	2.2	38	(0.67, 0.33)	ITO/HATCN/TAPC/CBP:TNZPPI (10 wt %)/TmPyPB/LiF/Al	Doped device, near-infrared emission, vacuum-deposited emissive layer.	Wan et al. ¹⁸

	6.96 (-)	3.71	~100	90.5	(0.153, 0.059)	ITO/NPB/TcTa/CBP: TPINCz (20 wt %)/TPBi/LiF/Al	Doped device, violet/blue emission, vacuum- deposited emissive layer.	Chen et al. ¹⁹
	1.47 (-)	0.20	91	28	(0.70, 0.30)	ITO/HATCN/TAPC/p -TPA-PT- CN/TmPyPB/LiF/Al	Non-Doped device, near- infrared emission, vacuum- deposited emissive layer.	Jiang et al. ²⁰
	5.74 (-)	2.89	76	71	(0.152, 0.054)	ITO/HATCN/TAPC/T CTA/TFPBI/TmPyPb/ LiF/Al	Non-Doped device, deep- blue emission, vacuum- deposited emissive layer.	Qiu et al. ²¹

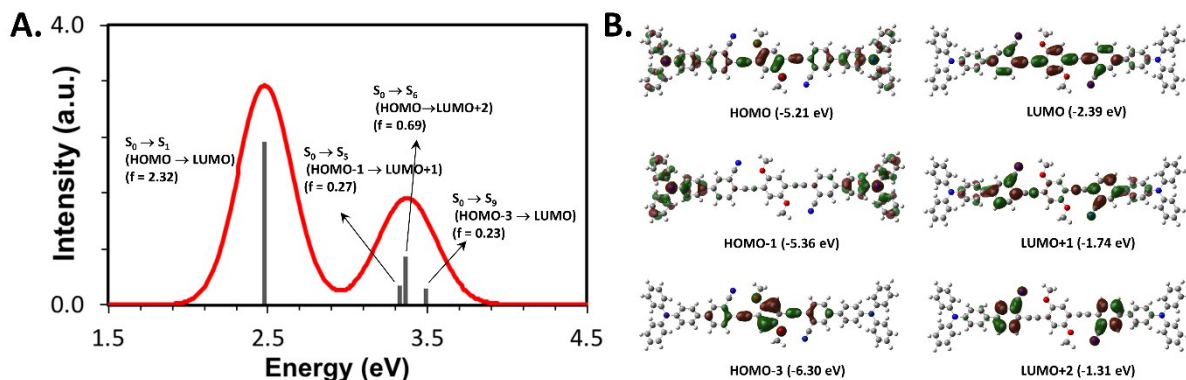
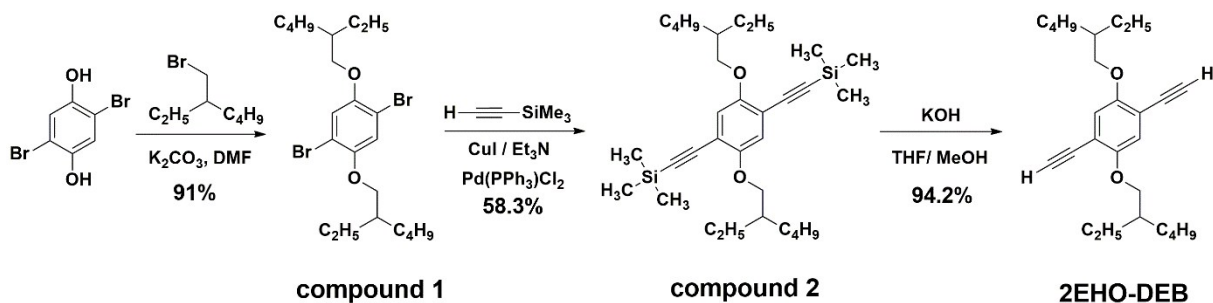


Figure S1. A. Calculated UV-Vis optical absorption spectrum for **2EHO-TPA-CNPE**. (The spectrum was obtained by using a 0.2 eV full-width-half-maximum (FWHM) Gaussian broadening to vertical levels) B. Canonical occupied (left) and virtual (right) molecular orbitals that are significantly involved in the low-lying excited states of **2EHO-TPA-CNPE**.



Scheme S1. Synthesis of 2EHO-DEB.

*Synthesis of 1,4-dibromo-2,5-bis(2-ethylhexyloxy)benzene (**compound 1**).* To a mixture of potassium carbonate (1.55 g, 11.18 mmol) and 2-ethylhexylbromide (3.02 g, 15.66 mmol) dissolved in 15 mL DMF, 2,5-dibromohydroquinone (1.50 g, 5.59 mmol) was slowly added under nitrogen. The resulting reaction solution was stirred at 100 °C for 48 h. The mixture was then cooled to room temperature and quenched with water. The reaction mixture was extracted with dichloromethane, and the organic phase was washed with water, dried over Na₂SO₄, filtered, and evaporated to dryness to give the crude product. The crude was then purified by column chromatography on silica gel using hexane as the eluent to give **compound 1** as a colorless oil (2.51 g, 91% yield). ¹H NMR (400 MHz, CDCl₃): δ 7.09 (s, 2H), 3.84 (d, 4H, *J*=4.0 Hz), 1.74-1.77 (m, 2H), 1.43-1.57 (m, 8H), 1.32-1.35 (m, 8H), 0.91-0.96 (m, 12H).

*Synthesis of 1,4-bis(ethynyltrimethylsilane)-2,5-bis(2-ethylhexyloxy)benzene (**compound 2**).*

A mixture of 1,4-dibromo-2,5-bis(2-ethylhexyloxy)benzene (2.5 g, 5.08 mmol), Pd(PPh₃)₂Cl₂ (0.214 g, 0.305 mmol), and CuI (0.049 g, 0.254 mmol) in Et₃N (50 mL) was stirred for ten minutes. Ethynyltrimethylsilane (1.247 g, 12.7 mmol) was then added, and the reaction mixture was heated at 90 °C under nitrogen for 48 h. Then, the reaction mixture was cooled to room temperature and filtered; the filtrate was evaporated to dryness to yield a crude mixture, which was then purified by column chromatography on silica gel using hexane:ethylacetate (30:1) eluent to yield **compound 2** as a yellow oil (1.56 g, 58.3% yield). ¹H NMR (400 MHz, CDCl₃): δ 6.89 (s, 2H), 3.82-3.87 (m, 4H), 1.72-1.75 (m, 2H), 1.44-1.58 (m, 8H), 1.27-1.34 (m, 8H), 0.91-0.96 (m, 12H), 0.26 (s, 18H).

*Synthesis of 1,4-bis(ethynyl)-2,5-bis(2-ethylhexyloxy)benzene (**2EHO-DEB**).* The suspension of 1,4-bis(ethynyltrimethylsilane)-2,5-bis(2-ethylhexyloxy)benzene (**compound 2**) (1.56 g, 2.96 mmol) and KOH (4.98 g, 88.8 mmol) in THF:methanol (9:1) (150 mL) was stirred at room temperature for 1 h. Next, the reaction mixture was quenched with water, and the resulting solution was extracted with dichloromethane. The organic phase was washed with water, dried over Na₂SO₄, filtered, and evaporated to dryness to yield **2EHO-DEB** as a brown oil (1.067 g, 94.2% yield). ¹H NMR (400 MHz, CDCl₃): δ 6.96 (s, 2H), 3.85 (d, 4H, *J* = 4.0 Hz), 3.32 (s, 2H), 1.75-1.78 (m, 2H), 1.46-1.57 (m, 8H), 1.27-1.34 (m, 8H), 0.91-0.96 (m, 12H).

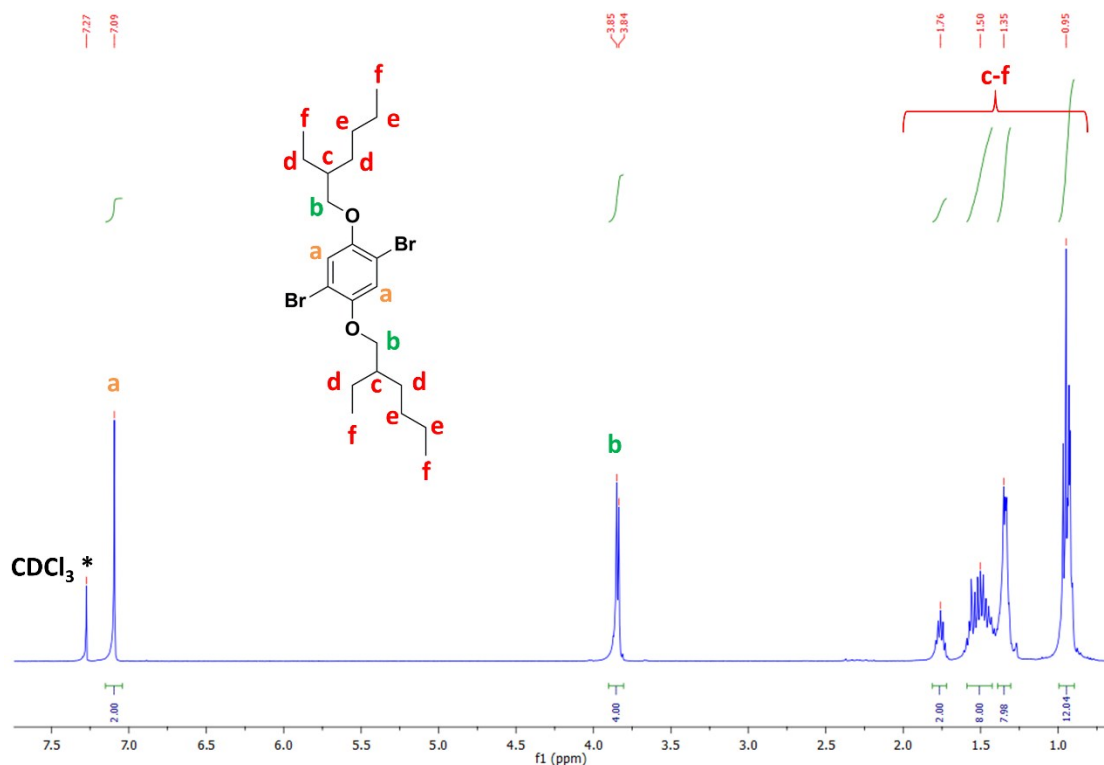


Figure S2. ^1H NMR spectra of compound **1** in CDCl_3 at room temperature.

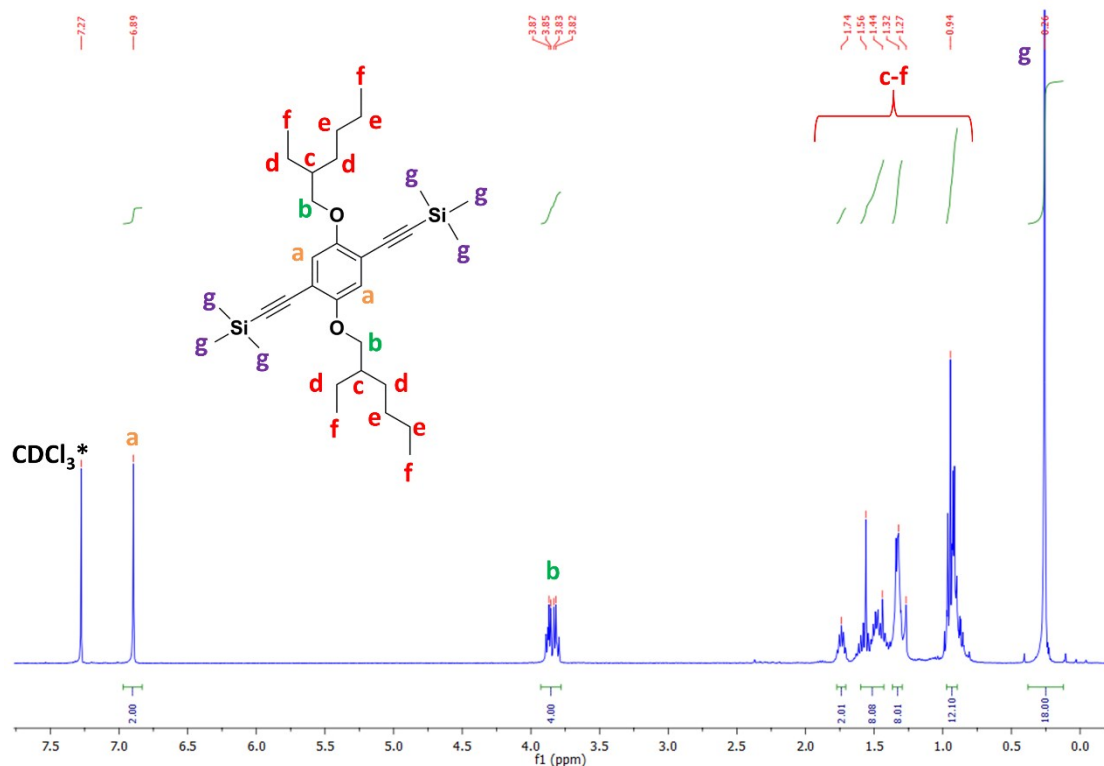


Figure S3. ^1H NMR spectra of compound **2** in CDCl_3 at room temperature.

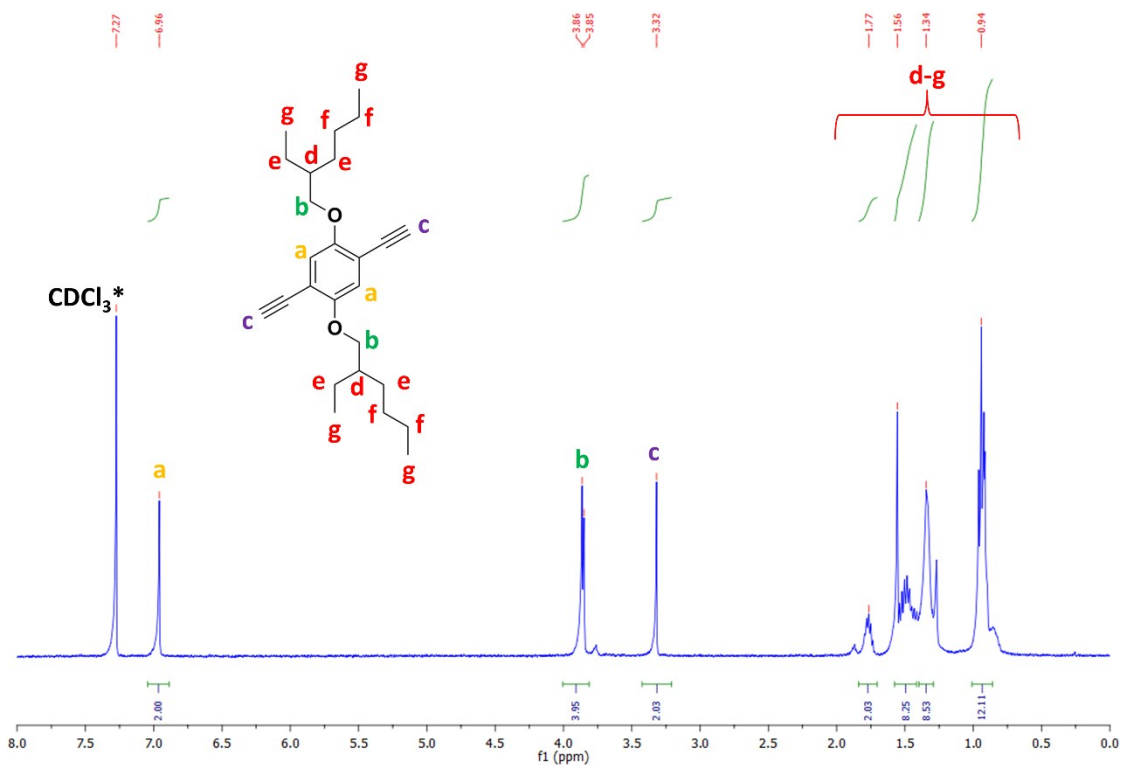


Figure S4. ^1H NMR spectra of 2EHO-DEB in CDCl_3 at room temperature.

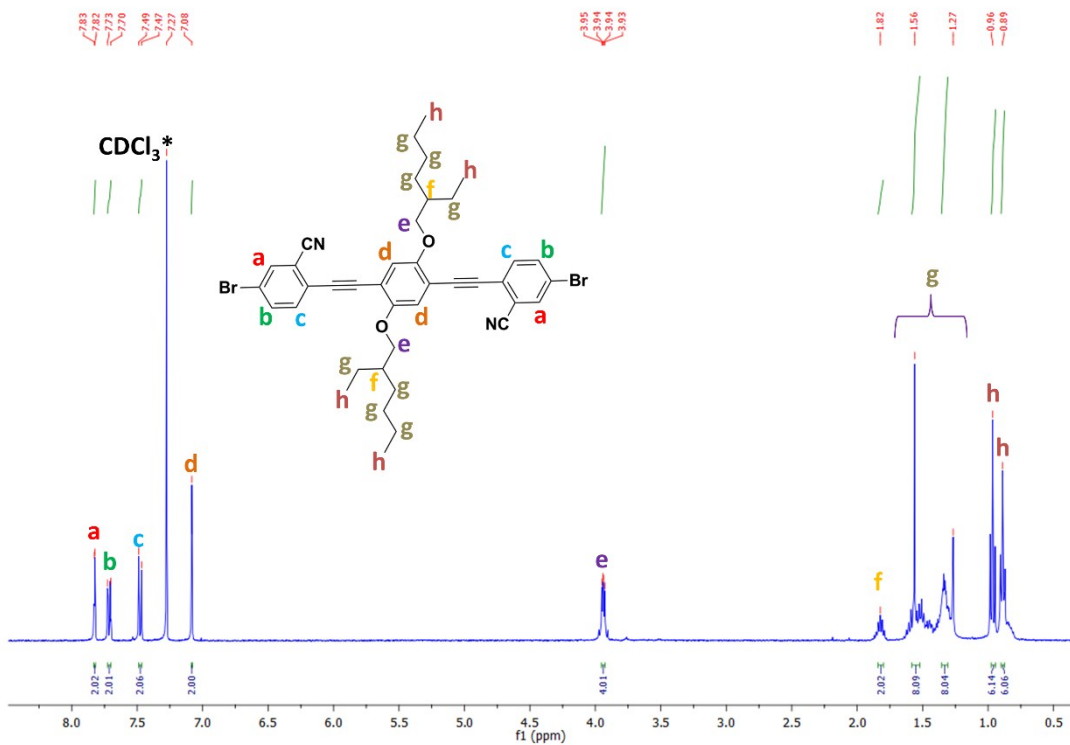


Figure S5. ^1H NMR spectra of **2**EHO-Br-CNPE in CDCl_3 at room temperature.

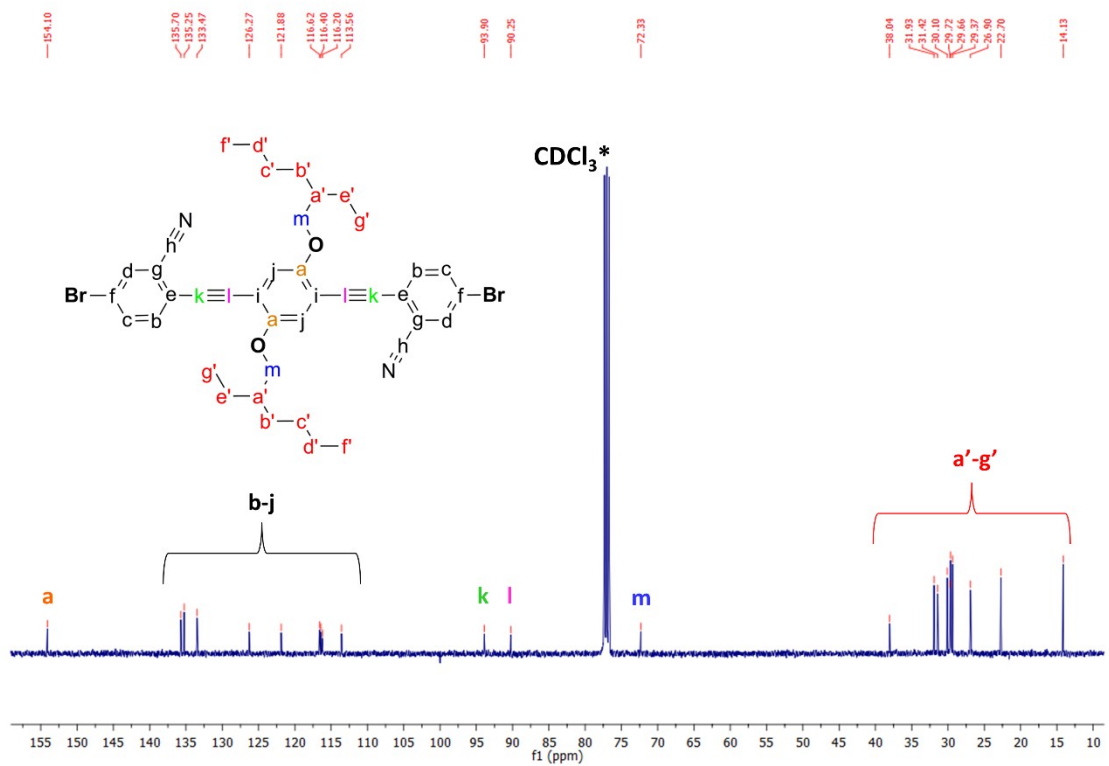


Figure S6. ^{13}C NMR spectra of 2EHO-Br-CNPE in CDCl_3 at room temperature.

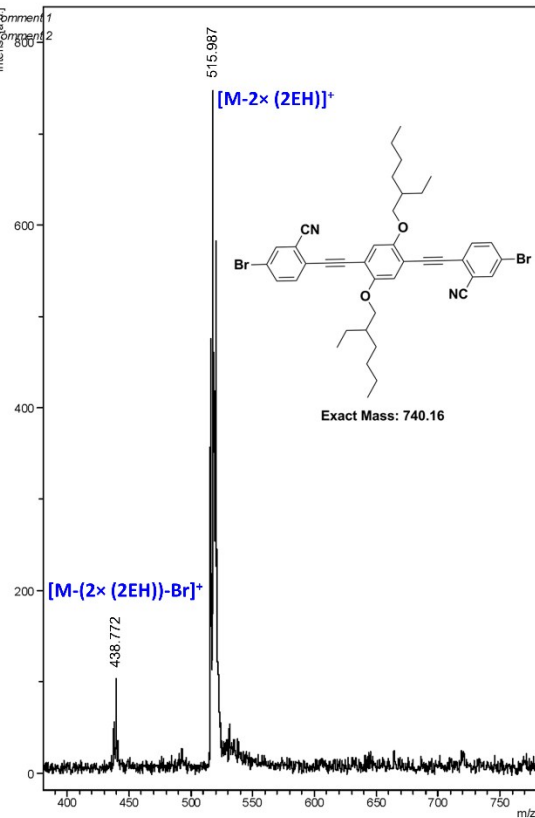


Figure S7. Positive ion and linear mode MALDI TOF-MS spectrum of 2EHO-Br-CNPE.

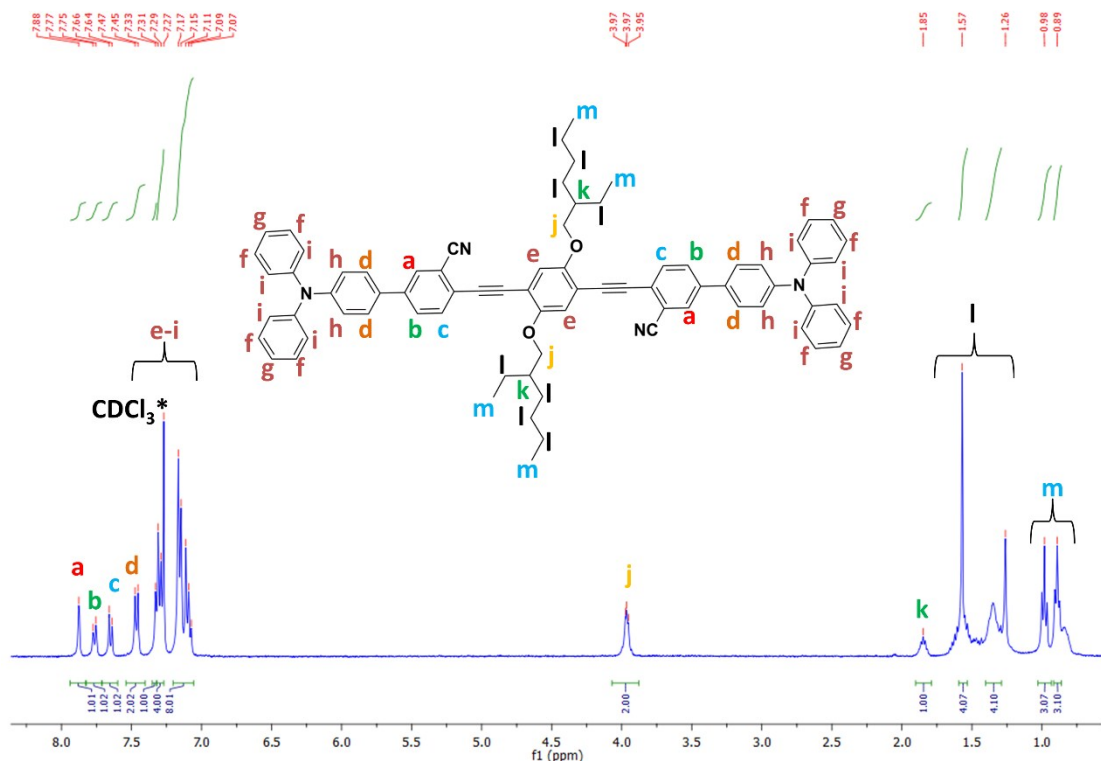


Figure S8. ^1H NMR spectra of **2EHO-TPA-CNPE** in CDCl_3 at room temperature.

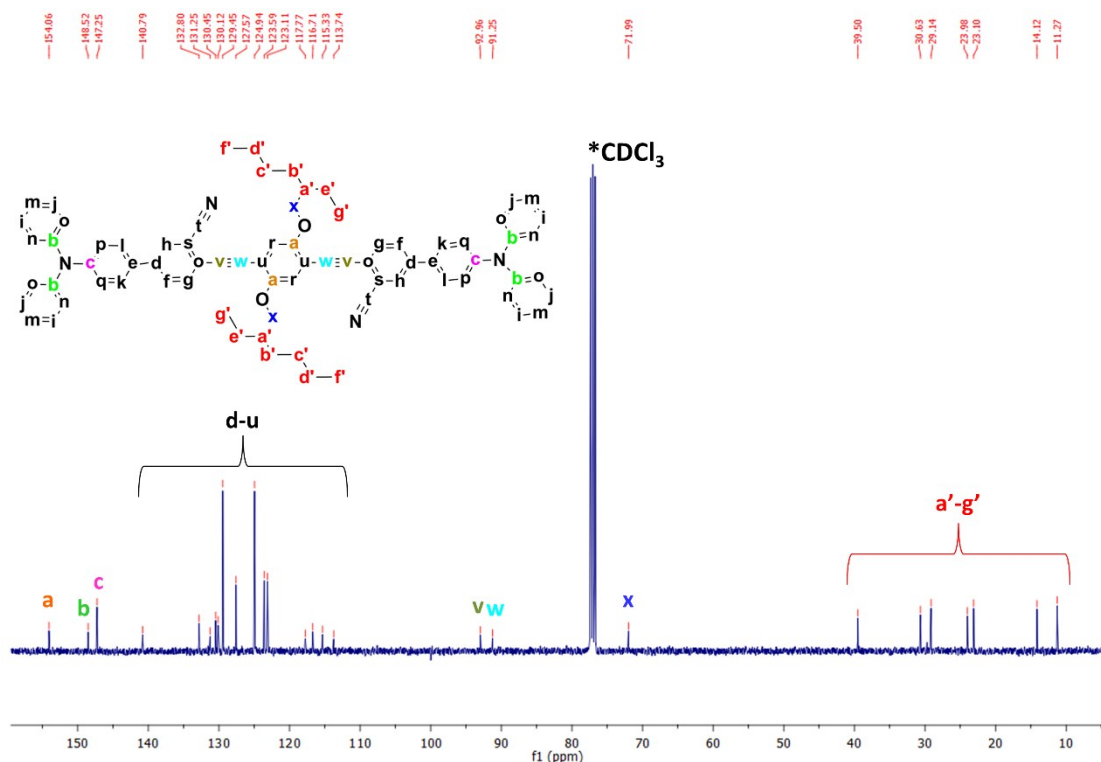


Figure S9. ^{13}C NMR spectra of **2EHO-TPA-CNPE** in CDCl_3 at room temperature.

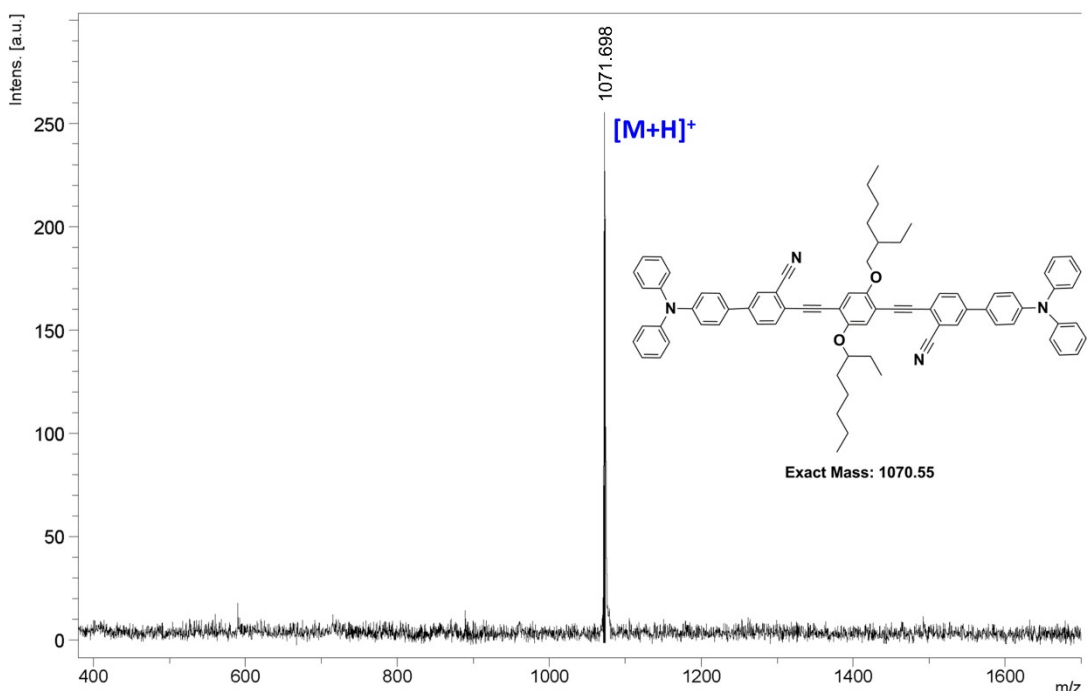


Figure S10. Positive ion and linear mode MALDI TOF-MS spectrum of **2EHO-TPA-CNPE**.

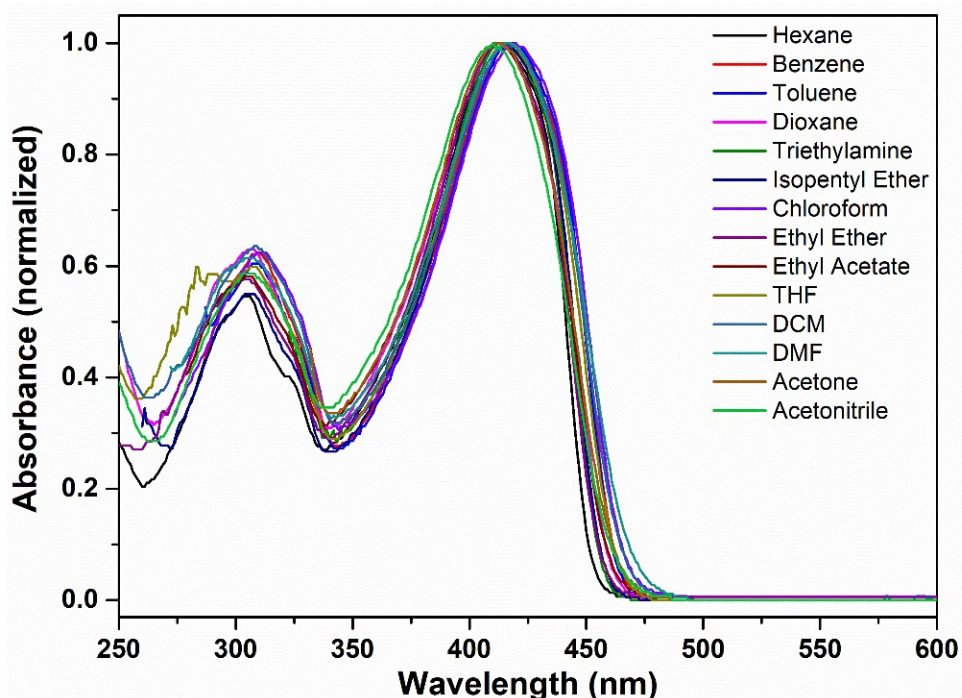


Figure S11. Solvatochromic optical absorption spectra of **2EHO-TPA-CNPE** in different solvents with increasing polarity (hexanes → acetonitrile). (The solvent orientational polarizability values ($f(\epsilon, n)$) are included in Table S2)

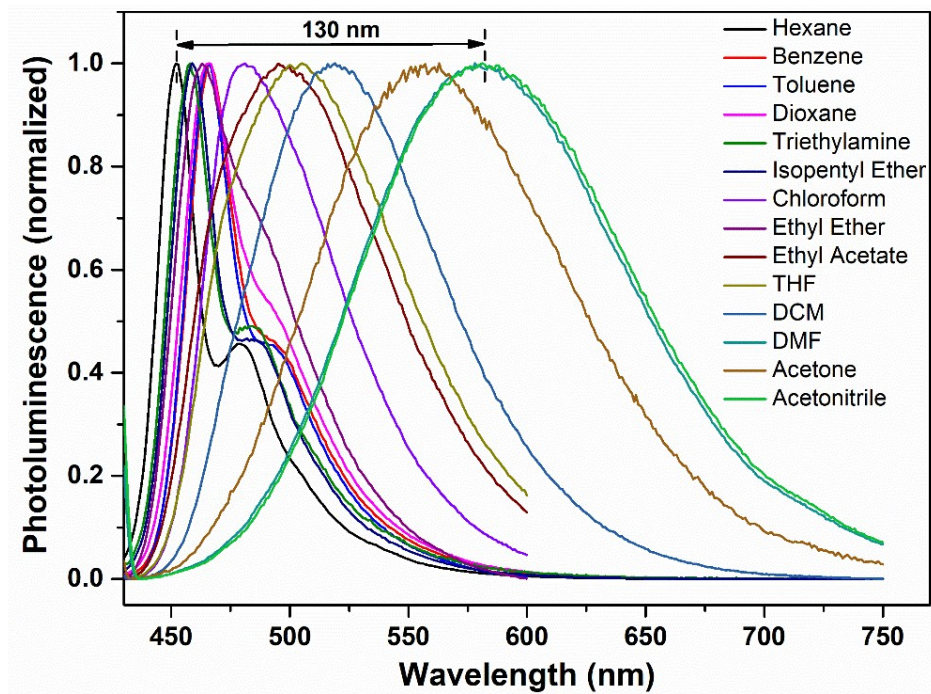


Figure S12. Solvatochromic photoluminescence spectra of **2EHO-TPA-CNPE** in different solvents with increasing polarity (hexanes → acetonitrile). (The solvent orientational polarizability values ($f(\epsilon, n)$) are included in Table S2)

Table S2. Solvatochromic optical absorption/photoluminescence peak positions (λ_{abs}^{max} and λ_{fl}^{max}) and Stokes shifts ($\nu_{abs} - \nu_{fl}$) for **2EHO-TPA-CNPE** in different solvents with increasing polarity (hexanes → acetonitrile), and solvent orientational polarizability values ($f(\epsilon,n)$).

Solvents	$f(\epsilon,n)$	λ_{abs}^{max} (nm)	λ_{fl}^{max} (nm)	$\nu_{abs} - \nu_{fl}$ (cm ⁻¹)
Hexane	0.001	413	452	2089.19
Benzene	0.0026	417	466	2521.59
Toluene	0.014	419	466	2407.12
Dioxane	0.0214	413	466	2753.85
Triethylamine	0.048	415	458	2262.33
Isopentyl Ether	0.0747	416	459	2251.97
Chloroform	0.148	412	481	3481.82
Ethyl Ether	0.167	414	463	2556.32
Ethyl Acetate	0.200	413	495	4011.06
THF	0.210	416	502	4118.14
DCM	0.217	417	519	4713.0
DMF	0.276	417	577	6649.8
Acetone	0.284	412	557	6318.52
Acetonitrile	0.305	410	582	7208.11

The Solvatochromic Lippert-Mataga Model:

The Lippert-Mataga model is used according to the following equation to estimate the dipole moments of S₁ state:

$$\nu_a - \nu_f = \frac{2(\mu_e - \mu_g)^2}{hca^3} f(\varepsilon, n) + (\nu_a^0 - \nu_f^0) \quad (*)$$

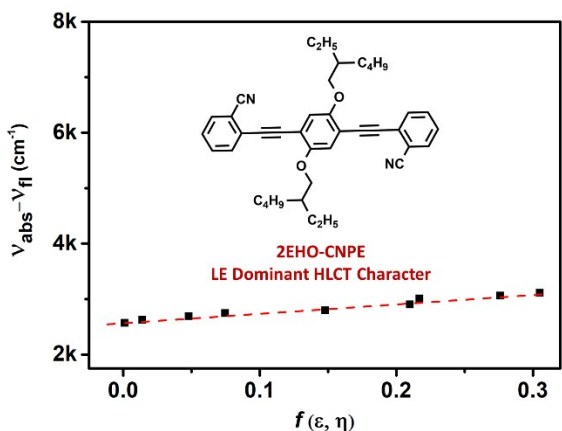
where h is Planck constant, c is the speed of light in vacuum, $\nu_a^0 - \nu_f^0$ is the Stokes shift when f is zero, μ_e and μ_g are dipole moments of excited state and ground state respectively. $f(\varepsilon, n)$ and a are the solvent orientation polarizability and the solvent Onsager cavity radius, respectively and can be calculated as follows:

$$f(\varepsilon, n) = \frac{\varepsilon - 1}{2\varepsilon + 1} - \frac{n^2 - 1}{2n^2 + 1}, \quad a = \left(\frac{3M}{4N\pi d}\right)^{1/3}$$

where ε is the solvent dielectric constant and n is the solvent refractive index. M is the molar mass, N is the Avogadro's constant, and d is the density of the solvents ($d = 1.0 \text{ g/cm}^3$).

$$\frac{2(\mu_e - \mu_g)^2}{hca^3}$$

In the Equation (*), $\frac{2(\mu_e - \mu_g)^2}{hca^3}$ is the term corresponding to the slope of the plot of Stokes shift $(\nu_a - \nu_f)$ versus the solvent orientation polarizability $f(\varepsilon, n)$. By estimating the dipole moments of ground state from density functional theory (DFT) calculations and the slope from the plot of $(\nu_a - \nu_f)$ vs $f(\varepsilon, n)$, we could calculate the dipole moments of excited state, μ_e .



Solvents	$f(\epsilon, \eta)$	$\lambda_{\text{abs}}^{\max}$ (nm)	$\lambda_{\text{fl}}^{\max}$ (nm)	$\nu_{\text{abs}} - \nu_{\text{fl}}$ (cm ⁻¹)
Hexane	0.001	388	431	2571.34
Toluene	0.014	388	432	2625.05
Triethylamine	0.048	387	432	2691.64
Isopentyl Ether	0.0747	387	433	2745.1
Chloroform	0.148	387	434	2798.32
THF	0.210	387	436	2904.01
DCM	0.217	387	438	3008.74
DMF	0.276	387	439	3060.75
Acetonitrile	0.305	387	440	3112.52

Figure S13. Solvatochromic Lippert-Mataga model for deep-blue emissive **2EHO-CNPE** showing the fitted linear correlation ($\nu_{\text{abs}} - \nu_{\text{fl}}$ vs. $f(\epsilon, \eta)$) and the corresponding optical absorption/photoluminescence data in different solvents with increasing polarity (hexanes → acetonitrile) (peak positions ($\lambda_{\text{abs}}^{\max}$ and $\lambda_{\text{fl}}^{\max}$), Stokes shifts ($\nu_{\text{abs}} - \nu_{\text{fl}}$), and solvent orientational polarizability values ($f(\epsilon, \eta)$)).

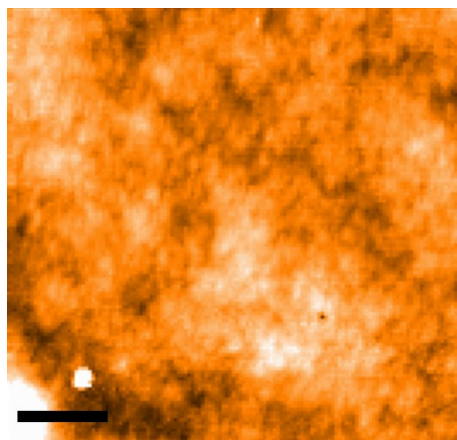


Figure S14. Atomic force microscopy (AFM) image of spin-coated and annealed (80 °C for 10 min) **2EHO-TPA-CNPE** thin-film (55 nm) on ITO/PEDOT:PSS(60 nm). The scale bar denotes 1 μm.

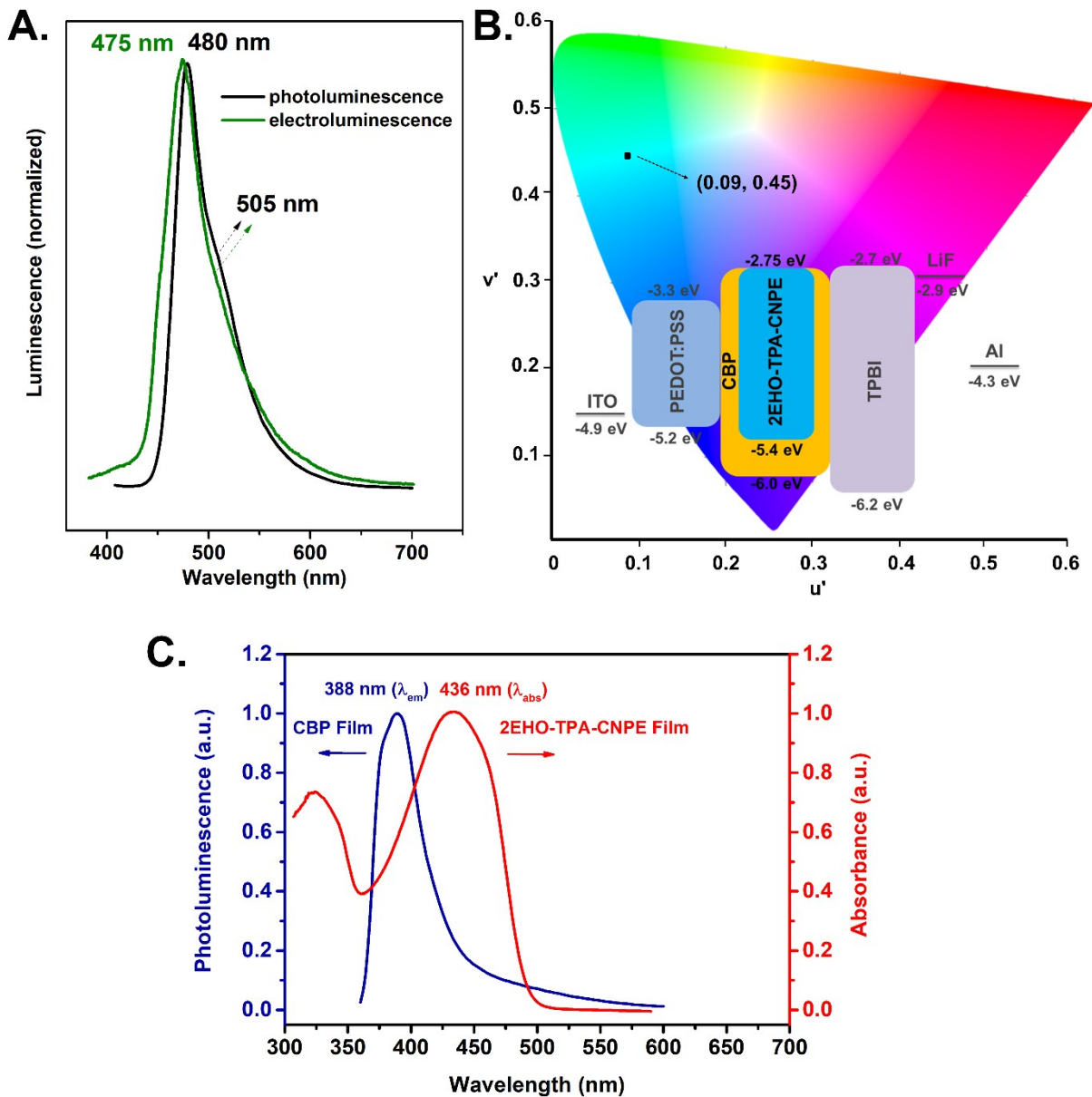


Figure S15. A. Photoluminescence spectra of spin-coated doped (4.0 wt % **2EHO-TPA-CNPE**) CBP thin-film and electroluminescence spectra (at 200 cd/m²) of the corresponding OLED device (ITO/PEDOT:PSS(60 nm)/CBP:**2EHO-TPA-CNPE**(60 nm)/TPBI(40 nm)/LiF(0.8 nm)/Al(100 nm)). B. Energy level diagram and CIE 1976 (u' , v') chromaticity diagram showing (u' , v') coordinates of the sky-blue emitting doped OLED device at 200 cd/m². C. Photoluminescence and absorption spectra of neat spin-coated CBP ($\lambda_{exc} = 355$ nm) and **2EHO-TPA-CNPE** thin-films, respectively, showing a good spectral overlap.

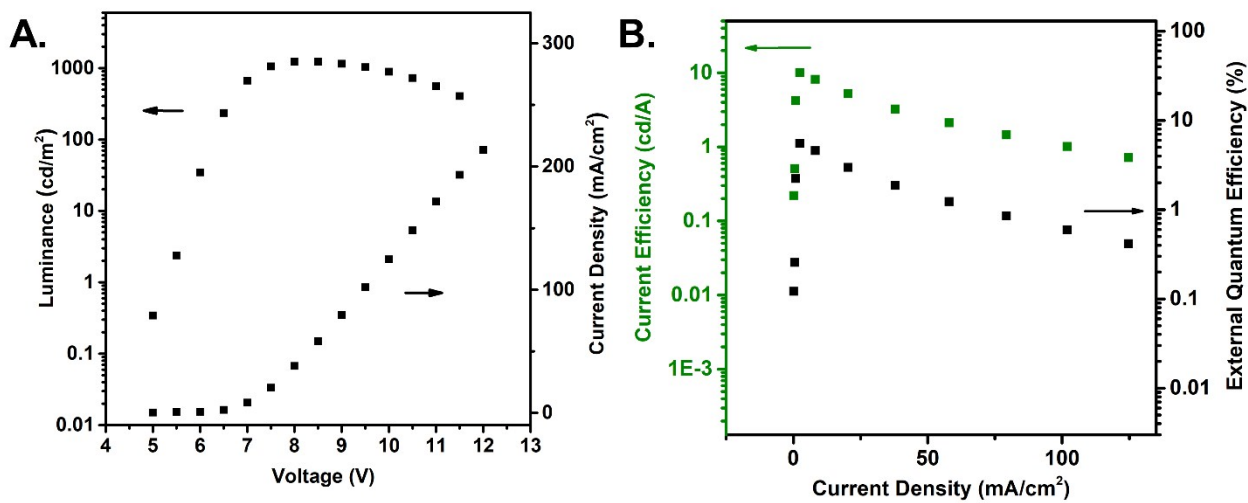


Figure S16. Luminance-voltage-current density (A) and current efficiency-current density-external quantum efficiency (B) plots for the doped OLED device (ITO/PEDOT:PSS(60 nm)/CBP:**2EHO-TPA-CNPE**(60 nm)/TPBI(40 nm)/LiF(0.8 nm)/Al(100 nm)).

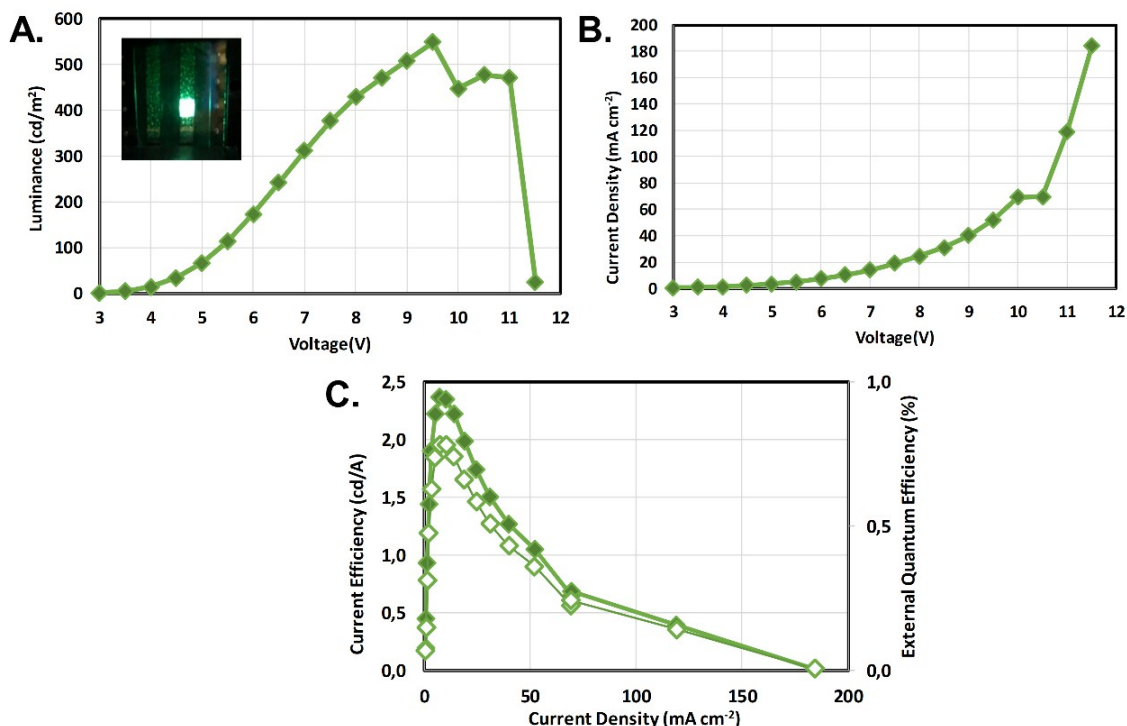


Figure S17. Luminance-voltage (A), current density-voltage (B), and current efficiency(closed symbols)-current density-external quantum efficiency (open symbols) (C) plots for the ink-jet printed OLED device (ITO/PEDOT:PSS(60 nm)/**2EHO-TPA-CNPE**(50 nm/ink-jet printed)/TPBI(40 nm)/LiF(0.8 nm)/Al(100 nm)).

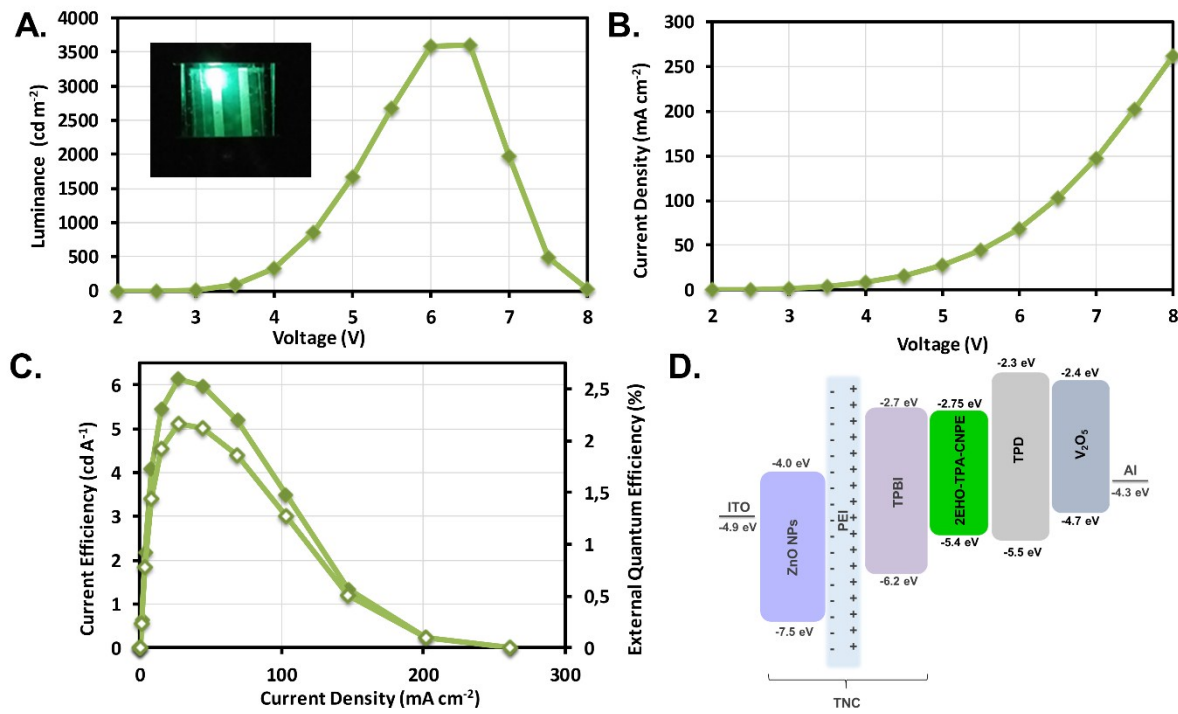


Figure S18. Luminance-voltage (A), current density-voltage (B), and current efficiency(closed symbols)-current density-external quantum efficiency (open symbols) (C) plots, and energy level diagram (D) for the inverted OLED device (ITO/TNC(50 nm)/**2EHO-TPA-CNPE**(55 nm)/TPD(50 nm)/V₂O₅(15 nm)/Al(100 nm)).

Table S3. Calculated energies, oscillator strengths, important configurations, and weights for the singlet/triplet excited states of **2EHO-TPA-CNPE**.

Excited State	Energy (eV)	Oscillator Strength (a.u.)	Configuration of Excited States in Canonical MO Basis	Weight
T ₁	1.84	0.00	HOMO→LUMO	0.67
			HOMO-2→ LUMO	0.21
T ₂	2.36	0.00	HOMO-1→ LUMO	0.49
			HOMO→ LUMO+1	0.28
S ₁	2.48	2.32	HOMO-4→ LUMO	0.10
			HOMO→LUMO	0.96
T ₃	2.52	0.00	HOMO-2→ LUMO	0.56
			HOMO-1→ LUMO+1	0.12
S ₂	2.74	0.00	HOMO→LUMO	0.11
			HOMO-1→ LUMO	0.98
T ₄	2.80	0.00	HOMO-1→ LUMO	0.35
			HOMO→ LUMO+1	0.27
T ₅	2.88	0.00	HOMO-2→ LUMO+1	0.16
			HOMO-3→ LUMO+1	0.72
S ₃	2.88	0.03	HOMO-2→ LUMO	0.96
S ₄	3.15	0.00	HOMO→ LUMO+1	0.94
S ₅	3.32	0.27	HOMO-1→ LUMO+1	0.92

$$\lambda = \left| \frac{\langle \Psi_S | H_{SO} | \Psi_T \rangle}{\Delta E_{ST}} \right|_2$$

Table S4. Predicted matrix elements for the coupling () between singlet and triplet states of **2EHO-TPA-CNPE** tabulated in [cm⁻¹/eV]². All calculations were done using ZORA Hamiltonian with perturbative spin-orbit coupling scheme and B3LYP/TZP level of theory.

	T ₁	T ₂	T ₃	T ₄	T ₅	T ₆	T ₇	T ₈	T ₉	T ₁₀
S ₁	0.00	0.01	0.14	0.61	0.01	0.00	0.27	0.01	0.09	0.02
S ₂	0.03	0.00	0.10	0.01	1.48	0.14	0.00	0.03	0.03	0.71
S ₃	0.00	0.06	0.00	1.20	0.35	0.00	0.26	0.00	0.20	0.02
S ₄	0.01	0.00	0.00	0.00	0.45	13.32	0.11	37.39	0.86	18.87
S ₅	0.00	0.00	0.00	0.06	0.00	0.01	1.70	0.01	0.46	1.83
S ₆	0.00	0.02	0.00	0.04	0.00	0.02	0.72	0.01	0.53	0.21
S ₇	0.00	0.00	0.01	0.00	0.00	0.04	0.00	0.05	0.04	12.74
S ₈	0.01	0.00	0.05	0.00	0.05	0.34	0.06	0.23	0.00	9.22
S ₉	0.00	0.05	0.00	0.09	0.00	0.00	0.03	0.00	0.03	0.04
S ₁₀	0.01	0.01	0.12	0.00	0.15	1.24	0.52	1.51	0.00	0.02

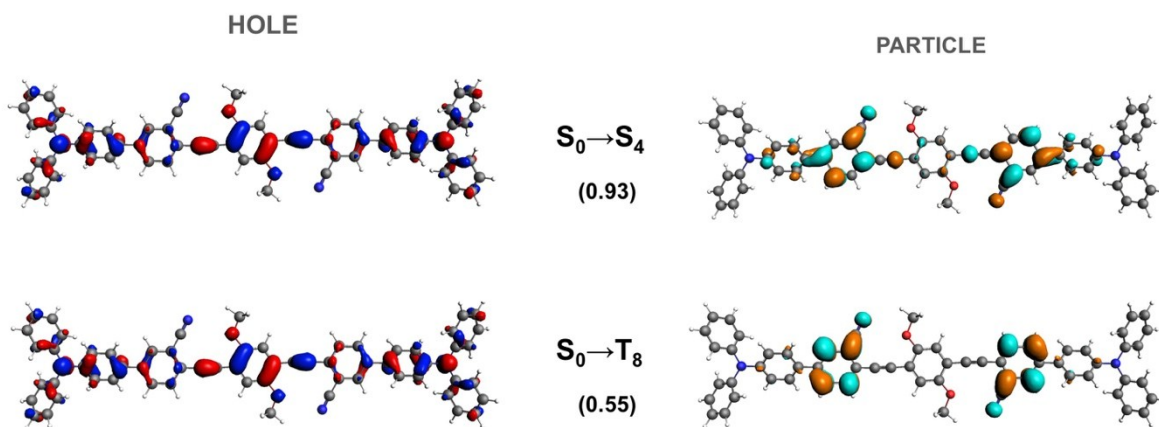


Figure S19. Natural transition orbitals of the S₄ and T₈ states, which show the largest spin-orbit facilitated coupling shown in Table S4 for RISC process. For these states, hole wave function is very similar whereas the particle wave functions exhibit a 90° rotation from singlet to triplet state, which is expected to produce a large spin-orbit coupling.

References

- 1 Y. Yu, L. Ma, Z. Feng, B. Liu, H. Zhou, H. Qin, H. Li, J. Song, G. Zhou and Z. Wu, *J. Mater. Chem. C*, 2019, **7**, 5604–5614.
- 2 J. Jayabharathi, S. Panimozhi and V. Thanikachalam, *RSC Adv.*, 2018, **8**, 37324–37338.
- 3 S. Zhang, L. Yao, Q. Peng, W. Li, Y. Pan, R. Xiao, Y. Gao, C. Gu, Z. Wang, P. Lu, F. Li, S. Su, B. Yang and Y. Ma, *Adv. Funct. Mater.*, 2015, **25**, 1755–1762.
- 4 W. Li, D. Liu, F. Shen, D. Ma, Z. Wang, T. Feng, Y. Xu, B. Yang and Y. Ma, *Adv. Funct. Mater.*, 2012, **22**, 2797–2803.
- 5 H. Zhang, J. Zeng, W. Luo, H. Wu, C. Zeng, K. Zhang, W. Feng, Z. Wang, Z. Zhao and B. Z. Tang, *J. Mater. Chem. C*, 2019, **7**, 6359–6368.
- 6 C. Wang, X. Li, Y. Pan, S. Zhang, L. Yao, Q. Bai, W. Li, P. Lu, B. Yang, S. Su and Y. Ma, *ACS Appl. Mater. Interfaces*, 2016, **8**, 3041–3049.
- 7 Y. Xu, X. Liang, X. Zhou, P. Yuan, J. Zhou, C. Wang, B. Li, D. Hu, X. Qiao, X. Jiang, L. Liu, S. Su, D. Ma and Y. Ma, *Adv. Mater.*, 2019, **31**, 1807388.
- 8 W. Li, Y. Pan, L. Yao, H. Liu, S. Zhang, C. Wang, F. Shen, P. Lu, B. Yang and Y. Ma, *Adv. Opt. Mater.*, 2014, **2**, 892–901.
- 9 W. Li, Y. Pan, R. Xiao, Q. Peng, S. Zhang, D. Ma, F. Li, F. Shen, Y. Wang, B. Yang and Y. Ma, *Adv. Funct. Mater.*, 2014, **24**, 1609–1614.
- 10 L. Yao, S. Zhang, R. Wang, W. Li, F. Shen, B. Yang and Y. Ma, *Angew. Chemie - Int. Ed.*, 2014, **53**, 2119–2123.
- 11 S. Zhang, W. Li, L. Yao, Y. Pan, F. Shen, R. Xiao, B. Yang and Y. Ma, *Chem. Commun.*, 2013, **49**, 11302–11304.
- 12 G. Li, J. Zhao, D. Zhang, J. Zhu, Z. Shi, S. Tao, F. Lu and Q. Tong, *New J. Chem.*, 2017, **41**, 5191–5197.
- 13 W. Z. Yuan, X. Bin, G. Chen, Z. He, J. Liu, H. Ma, Q. Peng, B. Wei, Y. Gong, Y. Lu, G. He and Y. Zhang, *Adv. Opt. Mater.*, 2017, **5**, 1700466.
- 14 C. Li, M. Hanif, X. Li, S. Zhang, Z. Xie, L. Liu, B. Yang, S. Su and Y. Ma, *J. Mater. Chem. C*, 2016, **4**, 7478–7484.
- 15 C. Fu, S. Luo, Z. Li, X. Ai, Z. Pang, C. Li, K. Chen, L. Zhou, F. Li, Y. Huang and Z. Lu, *Chem. Commun.*, 2019, **55**, 6317–6320.
- 16 X. Tang, Q. Bai, Q. Peng, Y. Gao, J. Li, Y. Liu, L. Yao, P. Lu, B. Yang and Y. Ma, *Chem. Mater.*, 2015, **27**, 7050–7057.
- 17 X. Han, Q. Bai, L. Yao, H. Liu, Y. Gao, J. Li, L. Liu, Y. Liu, X. Li, P. Lu and B. Yang, *Adv. Funct. Mater.*, 2015, **25**, 7521–7529.
- 18 Q. Wan, J. Tong, B. Zhang, Y. Li, Z. Wang and B. Z. Tang, *Adv. Opt. Mater.*, 2020, **8**, 1901520.
- 19 W.-C. Chen, Y. Yuan, S.-F. Ni, Q.-X. Tong, F.-L. Wong and C.-S. Lee, *Chem. Sci.*, 2017, **8**, 3599–3608.

- 20 J. Jiang, X. Li, M. Hanif, J. Zhou, D. Hu, S. Su, Z. Xie, Y. Gao, B. Yang and Y. Ma, *J. Mater. Chem. C*, 2017, **5**, 11053–11058.
- 21 X. Qiu, S. Ying, C. Wang, M. Hanif, Y. Xu, Y. Li, R. Zhao, D. Hu, D. Ma and Y. Ma, *J. Mater. Chem. C*, 2019, **7**, 592–600.